Artefact-free color and contrast modification

Julien Rabin, Julie Delon, Yann Gousseau

Artefact-free color and contrast modification

Julien Rabin, Julie Delon and Yann Gousseau

***Abstract*—This work is concerned with the modification of the gray level or color distribution of digital images. A common drawback of classical methods aiming at such modifications is the revealing of artefacts or the attenuation of details and textures. In this work we propose a generic filtering method enabling, given the original image and the radiometrically corrected one, to suppress artefacts while preserving details. The approach relies on the key observation that artefacts correspond to spatial irregularity of the so-called *transportation map*, defined as the difference between the original and the corrected image. The proposed method draws on the non-local Yaroslavsky filter to regularize the transportation map. The efficiency of the method is shown on various radiometric modifications: contrast equalization, midway histogram, color enhancement and color transfer. A comparison with related approaches is also provided.**

***Index Terms*—contrast modification, color transfer, contrast adjustment, contrast equalization, histogram specification, optimal transportation, image regularization, artefact-free.**

I. Introduction

APPLYING contrast changes to digital images is one of the most elementary tool for image enhancement. Such changes may be obtained by applying a prescribed function to the gray values of images, as in contrast stretching or Gamma correction, or by prescribing the histogram of the resulting image, as in histogram equalization or specification from an example image [1]. Such operations are characterized by the way they affect the histogram of an image and may be seen as modifications of their gray level distribution. These techniques extend to color images by considering a luminance channel, as in Gamma correction, or by working on each color channel separately. The prescription of the three-dimensional color distribution is more satisfying because it avoids the creation of false colors, but is also more involved. Actually, a nice theoretical framework enabling to merge the gray level and color cases is the one of optimal transportation, also known as the Monge-Kantorovich problem [2], as we will briefly recall in this paper. When the resulting color histogram is prescribed by a target image, one speaks of *color transfer*. Various approaches to this task are proposed in [3], [4], [5], [6].

Applications of contrast or color changes are of course extremely numerous. With the popularization of digital photography, these techniques have became immensely popular through the use of various "curves" in image editing software. Early uses of contrast equalization are the enhancement of medical images [7] and the normalization of texture for analysis purposes [8]. In a related direction, the construction of *midway* histograms [9], [10] is useful for the comparison of two images of the same scene. More recently, extensive campaigns of old movies digitization have claimed for the development of contrast modification techniques to correct flicker [11], [12]. Similar techniques are commonly used in the post-production industry [13], [14]. Another field of increasing industrial interest in which contrast changes play a central role is the one of imaging in bad climatic conditions, see e.g. [15]. Color modification or transfer is also useful for a wide range of applications: aquatic robot inspection [16], space image colorization [17], enhancement of painting images, etc.

A common drawback of most methods aiming at modifying the contrast or color content of images is their strong tendency to create visual artefacts. Indeed, when increasing the contrast, parasite structures that were barely visible become prominent. Most noticeable is the enhancement of noise and compression scheme patterns, such as "block effect" due to the JPEG standard. In the other direction, contrast reduction or color transfer may yield detail loss and texture washing. A last artefact is particularly noticeable in the case of color transfer and appears when the proportions of colors are very different between images. The goal of this paper is to propose a generic method for the correction of these artefacts.

Before proceeding, we now recall some of the approaches that have been proposed in the literature to suppress artefacts due to contrast or color modification. The simplest one is proposed in [18] in the context of local histogram modifications, and amounts to limit the modification depending on gradient values. While improving the results in some cases, this approach let most artefacts untouched. In [5], it is proposed to correct color transfer artefacts by using a variational regularization after the transfer. Still in a variational framework, the authors of [10] propose a unified formulation containing both color transfer and regularity constraints in a single energy minimization. For the problem of color proportion, a possible approach is to transfer color after having identified some homogeneous regions, as proposed in [19], [6]. A related class of works takes interest in the avoidance of compression artefacts, usually using the properties of the compression scheme, see e.g. [20].

In this paper, we propose to remove all the artefacts described above by regularizing the *transportation map*, defined as the image of the differences between the original image and the one after contrast or color modification. Indeed, we will show that all these artefacts may be interpreted as **spatial irregularities** of this *transportation map*. In order to regularize this map without introducing blur in the final image, we take inspiration from non-local methods [21] that have been proposed for image denoising and more precisely from

Julien Rabin is with CEREMADE, Université Paris Dauphine, Place du Maréchal De Lattre De Tassigny, 75775 Paris, Cedex 16.
E-mail: rabin@ceremade.dauphine.fr
Julie Delon and Yann Gousseau are with LTCI CNRS, Télécom ParisTech, 46 rue Barrault, 75634 Paris, Cedex 13.
E-mail: {delon,gousseau}@telecom-paristech.fr

the Yaroslavsky filter [22]. The transportation map is filtered by averaging pixel values using weights that are computed on the original image, therefore adapting to the geometry of this initial image. It will be shown that artefacts are progressively suppressed by iterating this filtering stage and that the proposed filter generally provide better results than the approaches described in the previous paragraph.

The paper is organized as follows. In Section II the general setting for contrast and color modifications is introduced. The generic approach proposed in this work is given in Section III and experiments are displayed in Section IV. In the appendices, useful facts and results about optimal transportation and powers of stochastic matrices are given.

II. Color and contrast modification

In this section, we recall how color and contrast modifications can be applied to images and why they are likely to create visual artefacts.

A. Contrast or color distribution of an image

Let $u : \Omega \mapsto \mathbb{R}^n$ be a discrete image, with $n = 1$ for a gray level image, $n = 3$ for a color image, and where $\Omega \subset \mathbb{Z}^2$ is the bounded image domain. Assume that u takes its values in the set $\{y_1, \dots, y_P\} \subset \mathbb{R}^n$, then the gray level or color distribution of u is defined as

$$h_u = \sum_{i=1}^{P} h_i \delta_{y_i}, \tag{1}$$

where $h_i = \frac{1}{|\Omega|} |\{x \in \Omega;\ u(x) = y_i\}|$. When $n = 1$, we denote by H_u the cumulative distribution function of h_u. The distribution h_u is also called the gray level or color histogram of u and H_u is called its cumulative histogram.

B. Color and contrast modifications

It is usual to apply simple radiometric transformations to a gray level image in order to improve its contrast and level of details. Such transformations generally consist in an increasing function T, in order to preserve gray level ordering. The image u becomes $T(u)$, and its gray level distribution becomes $h_{T(u)} = \sum_{i=1}^{P} h_i \delta_{T(y_i)}$. Particular cases of such transformations are histogram stretching ($T(x) = ax + b$) or histogram clipping ($T(x) = \min(\beta, \max(\alpha, x))$), used for instance to improve visualization in satellite or medical imaging [7]. Another example is the function $T(x) = \log(1 + x)$, which is particularly useful to visualize images of Fourier transforms, or high dynamic range images [23]. Similar transformations can also be applied to the luminance channel of a color image (see an example of histogram clipping in Figure 1(j)).

In some cases, it is useful to assign to an image u a given target distribution f. This amounts to find a mapping T (called contrast or color transfer) such that the distribution of $T(u)$ is equal or at least close to f, *i.e.* such that

$$h_{T(u)} \simeq f. \tag{2}$$

Most of the time, the equality cannot be exactly satisfied. For instance, if $h_u = \delta_{\frac{1}{2}}$ (u is a constant image) and $f = \frac{1}{2}(\delta_0 + \delta_1)$, there is no mapping T such that the distribution of $T(u)$ is exactly f. T is thus generally chosen so that $h_T(u)$ be close to f in some sense.

For $n = 1$, Equation (2) can be satisfied in the sense that the cumulative distribution functions $H_{T(u)}$ and F coincide on the values taken by $T(u)$. This is always possible if F is continuous. If we add the constraint that T is increasing , the solution is given by

$$T = F^{-1} \circ H_u, \tag{3}$$

where F^{-1} is defined as $F^{-1}(t) = \inf\{\lambda \in \mathbb{R};\ F(\lambda) \geq t\}$. If f is a constant distribution on the range of u, Equation (3) yields the well known *histogram equalization*. More generally, if f is the gray level distribution h_v of another image v, then $T = H_v^{-1} \circ H_u$ is called *histogram specification*. These transformations can also be applied to the luminance channel of a color image (an example is displayed in Figure 1(b)). Some variants of this framework have been proposed to apply such equalization locally [18], [24] (see Figure 1(c) and 1(d)).

When $n \geq 2$, the interpretation of Equation (2) is less clear and the monotonic constraint cannot be used anymore to find an optimal mapping T. A naive solution, proposed in [3] in the case of color images, consists in applying an affine transformation to the color distribution of u in order to match the mean and variance of the color distribution f. If this elementary solution can be satisfying for cases involving images having similar and simple color distributions, it usually fails in general cases. In order to find a satisfying mapping in the general case, the problem must be seen in the framework of optimal transport, as described in more details in Appendix A. If $n = 1$, this framework leads to formulas similar to (3) for histogram equalization and specification. If $n \geq 2$, however, no analytic formulation can be found for the optimal mapping T. Such mappings can be estimated numerically, for instance by using the simplex algorithm. Most of the time, this estimation leads to expansive computations. In practice, a satisfying approximation can be computed by estimating iteratively 1D optimal mappings on random axes, as proposed in [5] and studied in [25] (an illustration is proposed in Figure 1(m)). The result is fast to compute, although not perfectly optimal in the sense of the Monge-Kantorovich transport problem described in Appendix B.

C. Visual artefacts

As it can be observed from the several examples provided in Figure 1, four major visual artefacts can be caused by contrast or color modifications:

- ▷ ***Noise enhancement:*** this happens if the variance of the noise in u increases after the application of T to u, as illustrated for instance in Figures 1(b) and 2(d) for histogram equalization.
- ▷ ***Compression artefacts:*** these artefacts appear when the original image u is the result of some compression scheme (e.g. JPEG) and when pixels with similar colors are mapped to different colors (see *e.g.* Figure 1(o)).
- ▷ ***Detail loss:*** this results from a reduction of contrast between u and $T(u)$, and can be observed for instance on the head of the bird in Figure 1(p).

▷ ***Color proportion inconsistencies:*** Ideally, the mapping T should be defined in such a way that pixels having similar colors in the original image are mapped to similar colors. However, this is unfeasible if the proportions of colors are very different in the original and the target distributions, as illustrated by Figure 1(q) and 6(i).

Our approach to remove these artefacts relies on the observation that they are all due to spatial irregularities of the *transportation map* of the image u, defined as $T(u) - u$.

III. A NEW REGULARIZATION APPROACH FOR TRANSPORTATION MAPS

Following the observations of the previous section, we propose to spatially filter the transportation map. The solution we chose is inspired from *non-local filters* [21]. This concept has been introduced for image denoising by Yaroslavsky [22]. Similar filters have been independently defined, as *SUSAN* [26] or the *Bilateral Filter* [27]. More recently, a somehow radical extension of this approach, the so-called "Non-Local Mean" filter [21] has been shown to outperform many approaches to image denoising. In what follows, we will make use of a variant of the Yaroslavsky filter to regularize transportation maps.

A. Transportation Map Regularization

Recall that $T(u)$ is the image after color or contrast modification. In what follows, we write $\mathcal{M}(u) := T(u) - u$ for the transportation map of image u. We propose to regularize it thanks to the operator Y_u, a weighted average with weights depending on the similarity of pixels in the original image u. The effect of this operator on an image $v : \Omega \mapsto \mathbb{R}^n$ with $n \geq 1$ is defined as

$$[\mathrm{Y}_u\, v] : x \in \Omega \mapsto \frac{1}{C(x)} \int_{y \in \mathcal{N}(x)} v(y)\ \cdot w_u(x,y)\, dy \qquad (4)$$
$$\text{with weights } w_u(x,y) = e^{-\frac{\|u(x)-u(y)\|^2}{\sigma^2}} ,$$

where $\|.\|$ stands for the Euclidean distance in $\mathbb{R}^n$, where $\mathcal{N}(x) = x + \mathcal{N}(0) \subset \Omega$, with $\mathcal{N}(0)$ a spatial neighborhood of 0, where σ is a tuning parameter of the method and $C(x)$ is the normalization constant $C(x) = \int_{y \in \mathcal{N}(x)} w_u(x,y) dy$.

Observe that if we apply Y_u to the image u, we obtain the Yaroslavsky filter [22]. If the weights also decrease as a function of the distance to x, Y_u becomes similar to the *cross bilateral filter* introduced in [28] for flash photographic enhancement.

The regularization of the image $T(u)$, referred to as *Transportation Map Regularization* (**TMR**), is then defined as $\mathrm{TMR}_u(T(u)) := u + \mathrm{Y}_u\, \mathcal{M}(u)$. Now, observe that this formulation can be divided in two terms :

$$\mathrm{TMR}_u(T(u)) = \underbrace{\mathrm{Y}_u\big(T(u)\big)}_{\text{filtering of image } T(u)} + \underbrace{u - \mathrm{Y}_u(u)}_{\text{image detail}} . \qquad (5)$$

First, the image $T(u)$ is filtered by a non-local operator Y_u, following the regularity of the image u. This operation attenuates noise, compression and color proportion artefacts but also the details of the image $T(u)$. The second operation performed by the TMR filter consists in adding the quantity $u_{details} = u - \mathrm{Y}_u(u)$, which can be considered as details of the original image (*e.g.* texture and fine structures). We will see in the experimental section that these two steps are very important to obtain a natural rendering of the image.

B. Properties

The previously defined filter has two nice properties which enable us to reduce the visual artefacts described in Section II-C.

First, observe that this filter leaves all the images $u + \lambda$, $\lambda \in \mathbb{R}^n$, unchanged. Moreover, if the application T consists in a multiplication by a positive constant α, then $\mathrm{TMR}_u(\alpha u) = \alpha u + (1-\alpha) \cdot u_{details}$. If $\alpha > 1$, the transfer T increases the contrast. In that case, the TMR filter reduces the noise contained in the image difference $u_{details}$. If $\alpha < 1$ the transfer T decreases the contrast and the TMR filter restore the lost details contained in $u_{details}$.

C. Iteration of TMR and convergence study

In practice, more than one iteration of the TMR filter is required to remove all the aforementioned artefacts. The image $T(u)$ after k iterations of the TMR filter can be written as follows:

$$\mathrm{TMR}_u^k(T(u)) := \mathrm{Y}_u^k\big(T(u) - u\big) + u ,$$

where Y_u^k refers to the recursive use of the Y_u filter. An illustration for histogram equalization is given in Figures 5(b) and 5(a), where the equalized image (Figure 1(b)) is regularized using respectively one and several iterations of the TMR filter.

The question is then how to choose the right number of iterations k and one may wonder what happens for large values of k. Studying the limit of Y_u^k when $k \to \infty$ boils down to the study of the limit of the powers of a matrix. Indeed, let us resize the discrete image u into a column vector v of size m. In this setting, the linear filter Y_u can be written as an $m \times m$ matrix A , whose coefficients are

$$A_{i,j} = \frac{w_u(i,j) \cdot \mathbb{1}_{j \in \mathcal{N}(i)}}{\sum_{k=1}^m w_u(i,k) \cdot \mathbb{1}_{k \in \mathcal{N}(i)}} , \ 1 \leq i,j \leq m. \qquad (6)$$

In this formulation, i is the index in the vector v of a pixel x in u, and $\mathcal{N}(i)$ is the set of indexes in v corresponding to the 2D neighborhood $\mathcal{N}(x)$ in u. If we resize the map $T(u) - u$ into the vector w, then $\mathrm{Y}_u^k(T(u) - u)$ corresponds to the vector $A^k w$. Now, observe that the matrix A is stochastic, *i.e.* that $A_{i,j} \geq 0$, $\forall i,j$ and $\sum_{j=1}^m A_{i,j} = 1$, $\forall i$. If we assume that A is primitive, *i.e.* that A^r is strictly positive for some $r \in \mathbb{N}^*$ (and this is clearly true if the neighborhoods $\mathcal{N}(x)$ are disks of radius $\rho > 1$ in Equation (4)), the Perron-Frobenius theorem permits to conclude that A^k tends toward a stochastic matrix A^∞ when $k \to +\infty$, and that all the lines of A^∞ are equal (see Appendix B). This means that the map $\mathrm{Y}_u^k(T(u) - u)$ tends toward a constant image $\mathrm{Y}_u^\infty(T(u) - u)$. In other words, the limit image $\mathrm{TMR}_u^\infty(T(u))$ is only a shift of the image u by a constant color.

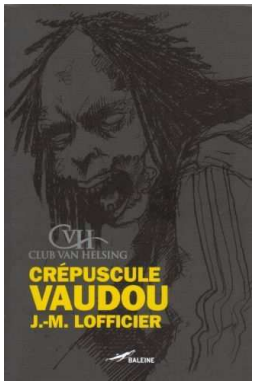

(a) Original image

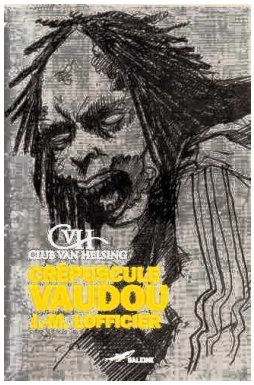

(b) Histogram equalization

(c) Spatial adaptive histogram equalization [18]

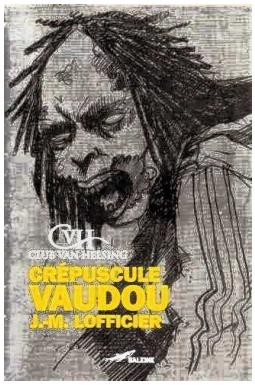

(d) Shape preserving equalization [24]

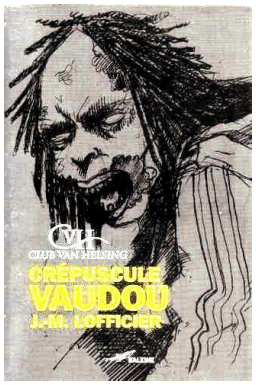

(e) Histogram clipping

(f) Top: Zoom of image (b). Bottom: Effect of TMR filter

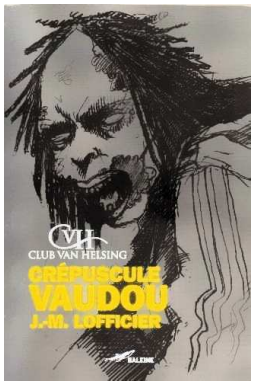

(g) Iterated TMR filter on image (b)

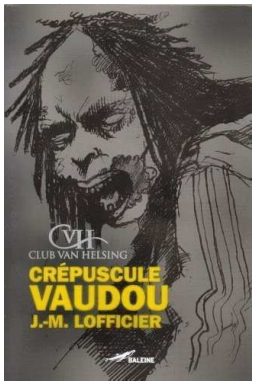

(h) Iterated TMR filter on image (c)

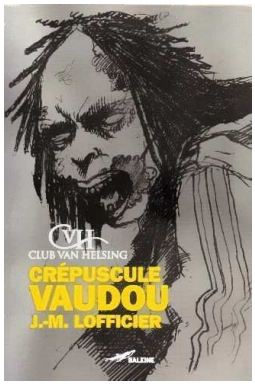

(i) Iterated TMR filter on image (d)

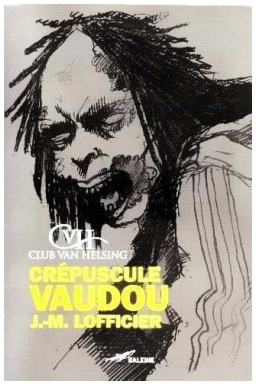

(j) Iterated TMR filter on image (e)

(k) Original image.

(l) Target color distribution.

(m) Raw color transfer.

(n) Iterated TMR filter on image 1(m).

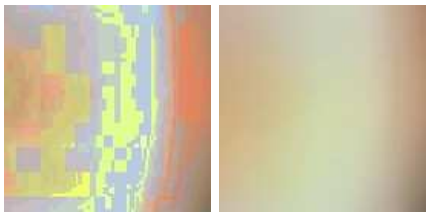

(o) Left: Details from image 1(m). Right: effect of TMR on JPEG artefacts.

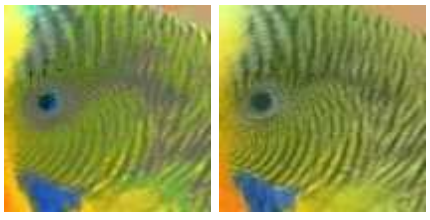

(p) Left: Details from image 1(m). Right: effect of TMR on fine detail loss.

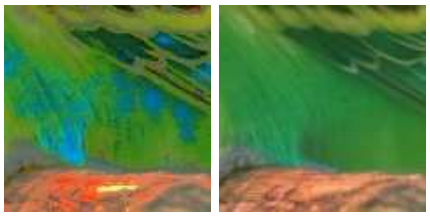

(q) Left: Details from image 1(m). Right: effect of TMR on color proportion artefacts.

Fig. 1. **Examples of visual artefacts produced by different image processing techniques and the corresponding regularizations.** The first row exhibits several images resulting from different contrast enhancement methods applied to the same original image (Figure 1(a)). The second row shows the corresponding applications of the TMR filter proposed in this paper. The third row shows an example of color transfer (colors of Figure 1(l) are affected to Figure 1(k)). Resulting artefacts are visible on Figure 1(m) and are shown to be removed by the TMR filtering in Figure 1(n). The fourth row shows corresponding details illustrating the various artefacts and their removal.

The Perron-Frobenius theorem also gives information on the convergence rate of A^r towards A^∞. More precisely, we know that $A^r - A^\infty$ behaves as $O(|\lambda|^r r^{m(\lambda)-1})$, where λ is the eigenvalue of A with the second largest modulus and where $m(\lambda)$ is the algebraic multiplicity of λ. In practice, $|\lambda|$ is generally close to 1 for a similarity matrix A, and the resulting convergence rate is quite slow, as it will be confirmed in the experimental section. The aim of the next section is to propose a way to stop automatically the iterations of the filter TMR.

D. Stopping criterion

In order to control the iterations of the TMR filter, we compute at each iteration a *convergence map*, written $\mathcal{C}$ and defined at each pixel as follows:

$$\mathcal{C}(x) = \| \, \mathrm{Y}_u^k \, \mathcal{M}\big(u(x)\big) - \mathrm{Y}_u^{k-1} \, \mathcal{M}\big(u(x)\big) \, \| \, ,$$

where $\|.\|$ is the average Euclidean norm in $\mathbb{R}^n$. We then consider that there is numerical convergence in pixel x when $\mathcal{C}(x) < t$, and the TMR filter is only applied to pixels for which the convergence map is greater than the threshold t. In all experiments, the convergence threshold has been set equal to $t = 1$ (for $n \times 8$-bit images).

In practice, if x is the first pixel to attain this numerical convergence, this boils down to replace the line corresponding to x in matrix A by the same line in the identity matrix. The new matrix A_1 is then iterated until a second pixel attain numerical convergence, and A_1 is then replaced by A_2, etc. Observe that each matrix A_j is stochastic and such that A_j^k converges when $k \to +\infty$ (see Appendix C for a proof), which implies that a new pixel attains numerical convergence after a finite number k_j of iterations. The whole process hence stops once all pixels are in $\mathcal{C}(x)$. At the end, if v is the vector corresponding to $T(u) - u$, we get

$$v^\infty = A_{n-1}^{k_{n-1}} \dots A_1^{k_1} A^{k_0} \cdot v \, . \tag{7}$$

Observe that the proposed stopping criterion permits also to save computation time since the iterations of the TMR filter concern fewer and fewer pixels.

IV. Experimental study

This section presents several applications of the TMR filter. Observe that this filter relies on two different parameters. The most important one is σ, which is used to compute the weighting terms in the computation of the regularized map (Formula (4)). In the following experiments, we have used $\sigma = 10$ The second parameter is related to the size of the neighborhood $\mathcal{N}(x)$. In experiments, we used disks of radius $\rho = 10$.

A. Convergence study

This paragraph illustrates the interest of the stopping criterion introduced in Section III-D. Consider the image u of Figure 2(a). This image has a narrow dynamic range, as illustrated by its histogram (Figure 2(b)). Applying an histogram equalization to u yields an image u_{eq} with a more satisfying dynamic range but also increases the noise level (Figure 2(d)). Using the stopping criterion proposed in Section III-D, 23 iterations of the TMR filter are required to converge in the sense of (7). This permits to reduce dramatically the noise level while preserving the contrast and details of u (Figures 2(e) and 2(m)).

The asymptotic behavior of the iterated TMR filter without using this stopping criterion is illustrated by the Figures 2(e) to 2(o). In accordance with the convergence study of Section III-C, we observe that the map $\mathrm{Y}_u^k(u_{eq} - u)$ tends toward a constant map $\mathrm{Y}_u^\infty(u_{eq} - u)$ [1] when k increases. The convergence rate is illustrated by Figure 2(c), which plots the values of the norm $\|\mathrm{TMR}_u^k(u_{eq}) - \mathrm{TMR}_u^\infty(u_{eq})\|$ when k increases. As expected, this convergence rate is very slow. This confirms that, while the threshold on the convergence is important in practice, its precise setting is not crucial.

B. Contrast modification

In this section, we investigate different applications of contrast modification to illustrate the interest of the proposed approach. In this context, we propose in Section IV-B3 a comparative study of our scheme with different regularization approaches that have been proposed in the literature.

1) Histogram modification: The first lines of Figure 1 illustrate the interest of the TMR filter for several contrast enhancement techniques, namely *histogram equalization* (Figures 1(b), 1(g)), *spatial adaptive histogram equalization* [18] (Figures 1(c), 1(h)) *shape preserving equalization* [24] (Figures 1(d), 1(i)) and *histogram clipping* (Figures 1(e), 1(j)). Notice how the artefacts described in Section II-C are present in these examples, in particular the enhancement of both noise and compression artefacts. In each case, the iterated TMR filter permits to remove these artefacts while preserving contrast and restoring details (see *e.g.* Figure 1(f)).

In Figure 3, a challenging example of contrast modification using both histogram clipping and Gamma correction is given, resulting in an increase of noise level. The result of the iterated TMR filter is illustrated in Figure 3(d), using $\sigma = 4$. Observe that our approach limits the noise enhancement and maintains the desired contrast modification. It should be noticed that using $\sigma = 10$ (see Figure 3(d)) on this example is not satisfying due to the very poor dynamic of the original image (Figure 3(a)). This illustrates that the practical choice of the parameter σ may depend on the considered contrast or color modification.

2) Flicker reduction: The proposed regularization scheme can also benefit the restoration of old movies. Figure 4(a) shows three images of a sequence suffering from a strong local flicker (fast and unnatural intensity fluctuations from one frame to the other). This sequence is restored by the local method proposed in [29] and the three corresponding restored frames are shown on Figure 4(b). The method manages to harmonize the local contrast in the sequence. However, as we can see, the flicker and film compression are so brutal that several artefacts appear on some parts of the frames (see for instance both heads in the second image and the jacket in

[1] The limit map can be computed explicitly in our case, see Appendix B.

(a) Original image u.

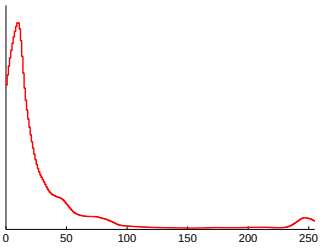

(b) Histogram of u.

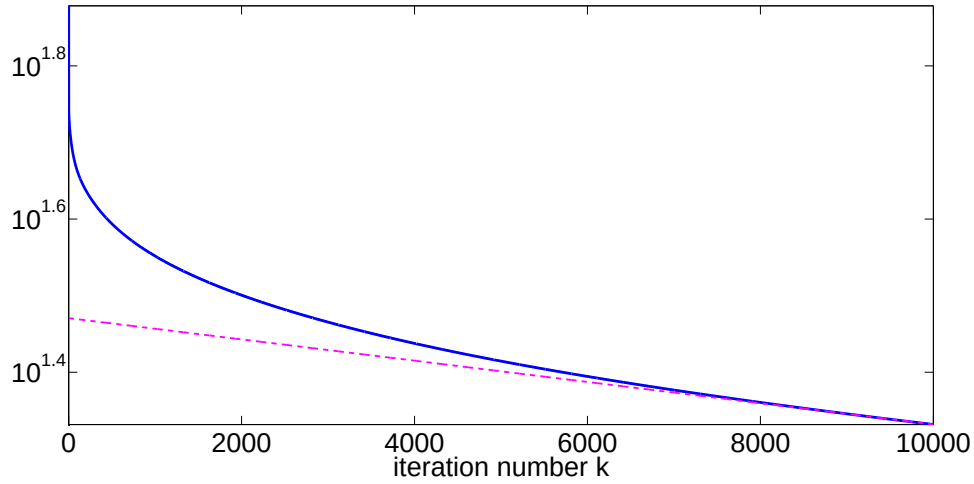

(c) Average Euclidean norm of difference $||\text{TMR}_u^k u_{eq} - \text{TMR}_u^\infty u_{eq}||$ as a function of the the number of iterations k.

(d) Equalization u_{eq}.

(e) $\text{TMR}_u^{23} u_{eq}$.

(f) $\text{TMR}_u^{10000} u_{eq}$.

(g) $\text{TMR}_u^{\infty} u_{eq}$

(h) Transportation map $u_{eq} - u$.

(i) Transportation map $\Upsilon_u^{23}(u_{eq} - u)$.

(j) Map $\Upsilon_u^{10000}(u_{eq} - u)$.

(k) Constant map $\Upsilon_u^{\infty}(u_{eq} - u)$.

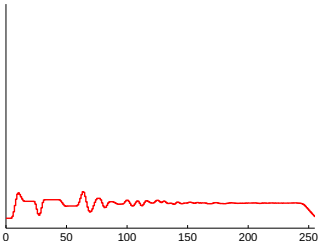

(l) Histogram of u_{eq}.

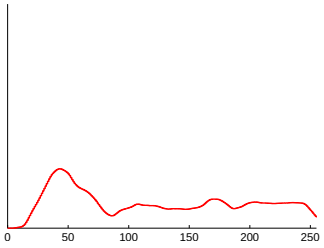

(m) Histogram of $\text{TMR}_u^{23} u_{eq}$.

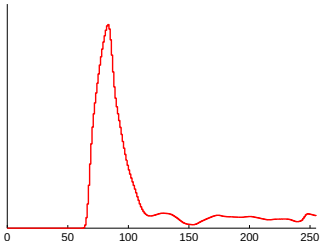

(n) Histogram of $\text{TMR}_u^{10000} u_{eq}$.

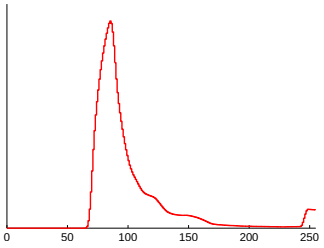

(o) Histogram of $\text{TMR}_u^{\infty} u_{eq}$.

Fig. 2. **Convergence study of the iterated TMR filter.** (a) a low dynamic range image u and (b) its gray level histogram; (d) image u_{eq}, obtained by applying an histogram equalization to u, and (l) histogram of u_{eq}; (h) the corresponding transportation map $\mathcal{M}(u) = u - u_{eq}$; (e) to (g) iterations of the TMR filter, with (e) 23 iterations (corresponding to the automatic stopping criterion), (f) 10000 iterations and (g) convergence; (m) to (o) the corresponding gray level histograms; (i) to (k) the corresponding transportation maps. Observe how the 23 iterations chosen by the stopping criterion permit to reduce the noise level while preserving contrast and image details.

the third image in Figure 4(b)). Figure 4(c) shows how these defects are corrected by the iterated TMR filter.

3) Comparison with other regularization approaches: In the following paragraphs, we confront our method with other approaches that have been proposed in the literature to reduce irregularities created by contrast modifications.

Gradient control: The approach of [18], that has been proposed to enhance the contrast of medical images, consists in applying local histogram equalizations independently on subparts of an image. We return to the images of Figure 1 to illustrate this point. Figure 1(c) shows an example where the image has been divided into 8-by-8 overlapping tiles. To

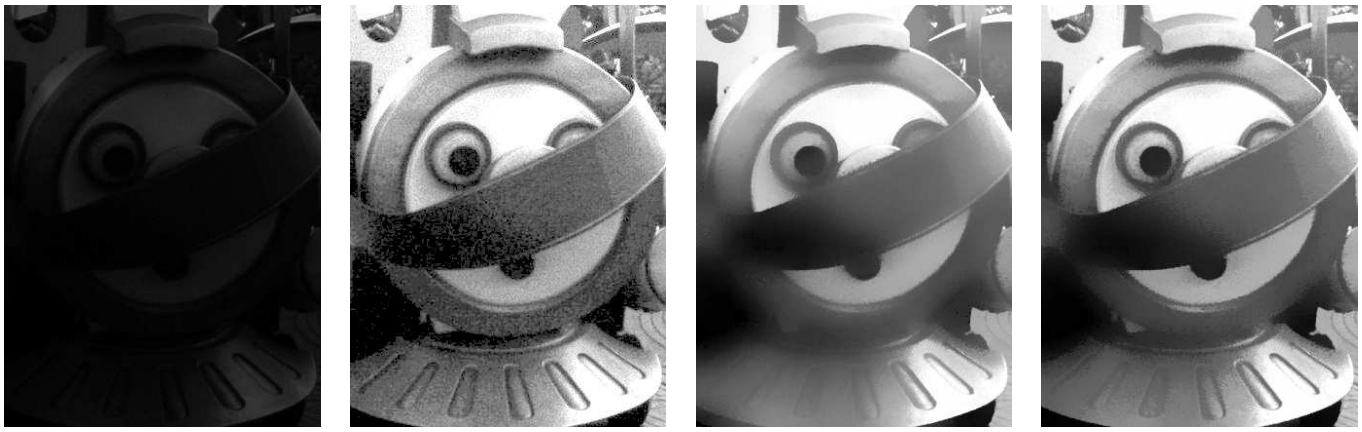

(a) Original image (b) Gamma correction (c) Iterated TMR filter with $\sigma = 10$ (d) Iterated TMR filter with $\sigma = 4$

Fig. 3. **Application of the iterated TMR filter for Gamma correction.** Figures 3(a) and 3(b): gray-level image and its contrast enhancement *via* histogram clipping and Gamma correction (with γ set to $\frac{1}{2}$). Figure 3(c) and 3(d): result of the iterated TMR filter, respectively with $\sigma = 10$ and $\sigma = 4$.

prevent the noise level to skyrocket (in particular in constant regions), the gradient of the transportation map is restricted to a user-defined interval, which also limits the contrast enhancement. In practice, one can observe that artefacts, if still present, are less noticeable than in the classical histogram equalization (Figure 1(b)). Figure 1(h) shows that the iterated TMR filter enables to remove the remaining artefacts while preserving the local contrast changes.

Two-scale decomposition technique: Figure 5(b) shows the result of a *single iteration* of the TMR filter when the mapping T is an histogram equalization (denoted here by the operator EQ) applied to the image u of Figure 1(a). Following (5), the resulting regularized image can be written as $\text{TMR}_u(\text{EQ}(u)) = \text{Y}_u \circ \text{EQ}(u) + u_{details}$, where $u_{details} = u - \text{Y}_u(u)$ is the detail image. This formulation shares similarity with the approach proposed in [23] in a different context for *tone mapping* (contrast reduction for high dynamic range images). In their framework, the image u is first decomposed into a base layer using the bilateral filter (corresponding here to $\text{Y}_u(u)$) and a detail layer $u_{details} = u - \text{Y}_u(u)$. A contrast reduction is then applied to the base layer, and $u_{details}$ is added to the result to obtain the final image. Figure 5(c) demonstrates that this approach, well suited for dynamic reduction, is not adapted to contrast enhancement, yielding discontinuities in flat regions.

One can see on Figure 5(a) how using iterations of the TMR filter until convergence yields even a better result. It is noticeable that this framework shares some common features with the two-scale decomposition approach introduced by Durand and Dorsay [23] in the case of *tone mapping* (contrast reduction for high dynamic range images).

Regraining: Another regularization scheme has been proposed by Kokaram *et al.* [5] as a post-processing for color transfer and can also be used for contrast modifications. This scheme relies on a variational formulation combining two fidelity terms: one depending on the gradient of images and the other one on their gray levels. The result of our implementation of their algorithm on the equalized image $\text{EQ}(u)$ is shown on Figure 5(d). Although the visual impact of artefacts is reduced, this method fails to restore completely details, yielding a blurred and "mottled" appearance.

C. Color transfer

This section presents the results of our regularization filter on several color transfer examples (see Section II-B). In all these experiments, the raw color transfer is computed thanks to the algorithm proposed in [5], which is both fast and easy to implement.

1) Four examples: We have already analyzed the color transfer example displayed at the bottom of Figure 1, which exhibits many artefacts (see details given in Figures 1(o), 1(p) and 1(q)). Figure 1(n) shows the result of several iterations of the TMR filter (until the stopping criterion is reached) on this example. As it can be observed on the different zooms, the regularization removes all compression artefacts while restoring fine details in the image and reducing color proportion problems.

Two additional examples of color transfer are proposed in Figure 6. The first one (Figure 6(a) to 6(f)) illustrates the two-terms decomposition of Equation (5). Let u denote the original image (Figure 6(a)) and $T(u)$ the same image after color transfer (Figure 6(c)), using the color palette of Figure 6(b). Then $\text{TMR}_u(T(u))$ (Figure 6(f)) can be seen as the sum of $\text{Y}_u(T(u))$ (Figure 6(d)), the filtered version of $T(u)$, and $u - \text{Y}_u(u)$ (Figure 6(e)), which restores the details of the original image u. In the second example, at the bottom of Figure 6, the colors of *Mahana no atua* by Gauguin are transferred to the painting *Le Déjeuner des Canotiers*, by Auguste Renoir. The resulting raw transportation map is shown on Figure 6(j), while Figure 6(k) and 6(l) show respectively the transportation map and the result of the color transfer after several iterations of TMR filter. Among other effects, the annoying color proportions problems (see for instance the blue spots on the white clothes) completely vanish, resulting in a far more plausible image.

A last example is given in Figure 7 to illustrate the versatility of the proposed approach for various color modification techniques. In this example, the image shown in Figure 7(a)

(a) Three consecutive frames from a movie [*Be Kind Rewind*, Michel Gondry, 2008], suffering from a strongly localized flicker.

(b) Same frames after local flicker reduction [29].

(c) Same frames after local flicker reduction and application of the TMR filter.

Fig. 4. **Application of the iterated TMR filter to flicker stabilization.** Figure 4(a): a sequence of three images corrupted by flicker (strong and fast local contrast change). Figure 4(b): flicker stabilization results with the method of Delon and Desolneux [29]. Observe that the contrast is well harmonized over the sequence, but some artefacts related to brutal and local contrast modifications appear. Figure 4(c): The iterated TMR filter permits to remove those artefacts.

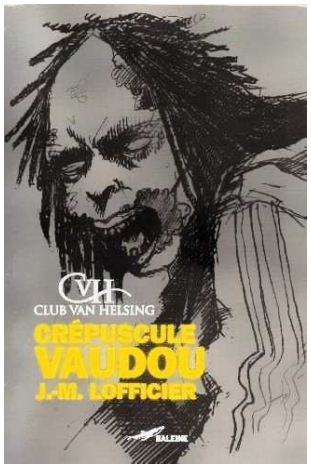

(a) Iterated TMR filter on $\mathrm{EQ}(u)$.

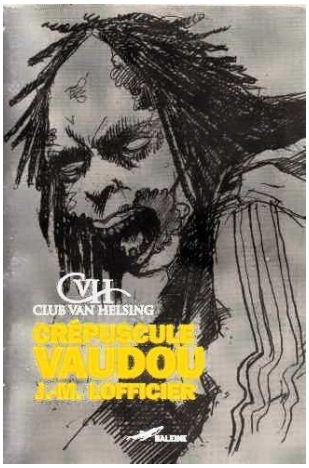

(b) One iteration of TMR on $\mathrm{EQ}(u)$: $\mathrm{Y}_u \circ \mathrm{EQ}(u) + u_{details}$.

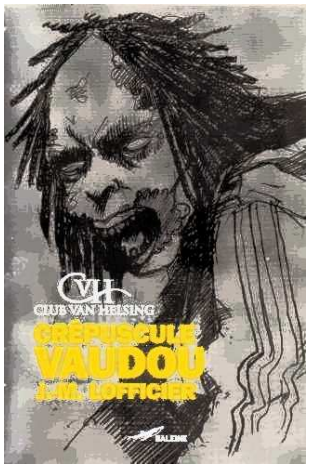

(c) Alternative approach: $\mathrm{EQ} \circ \mathrm{Y}_u(u) + u_{details}$.

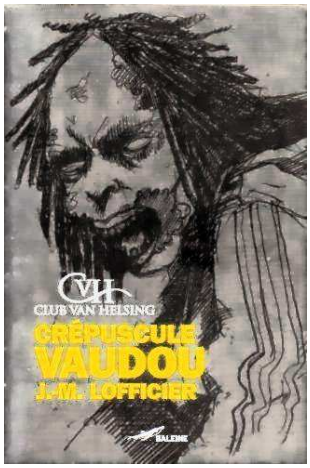

(d) Regraining [5] on $\mathrm{EQ}(u)$.

Fig. 5. **Comparison of the iterated TMR filter with other regularization techniques for contrast enhancement.** We consider here the image u and its equalization $\mathrm{EQ}(u)$ previously shown in Figures. 1(a) and 1(b)) respectively. In Figures 5(b) and 5(a), we show respectively one and several iterations of the TMR filter. The image $u_{details} = u - \mathrm{Y}_u(u)$ corresponds to the details extracted in u. One can compare results with a two-scale decomposition method inspired from [23] (Figure 5(c)) and with the "regraining" approach of [5] (Figure 5(d)). See Section IV-B3 for details.

(a) Original image. (b) Target color distribution. (c) Raw color transfer.

(d) Filtering of image (c). (e) Details extraction of (a). (f) Regularization of (c) with iterated TMR filter.

(g) Original image (Auguste Renoir, *Le déjeuner des Canotiers*, 1881). (h) Target color distribution (Paul Gauguin, *Mahana no atua – le jour de Dieu*, 1894). (i) Raw color transfer.

(j) Raw color transportation map. (k) Regularized color transportation map. (l) Iterated TMR filter.

Fig. 6. **Illustration of color transfer regularization with iterated TMR filter.** (see the electronic version of this paper). The first row displays (Figure 6(c)) the result of transferring the colors of Figure 6(b) to Figure 6(a). The second row illustrates that the corresponding regularization (Figure 6(f)) is obtained as the addition of the filtering of the raw color transfer (Figure 6(d)) with the details extracted from the original image (Figure 6(e)) where the mean has been changed for visualization purpose. The third row displays (Figure 8(a)) the result of transferring the colors of Figure 6(h) to Figure 6(g). The result of the proposed iterated TMR regularization is displayed in Figure 6(l). One observes that in contrast with Figure 6(i), the artefacts due to different color proportions are mostly removed. For illustration, the transportation maps before and after regularization are displayed in Figure 6(j) and 6(k) respectively.

is modified using an image editing software (The Gimp) to separately increase both the contrast and the saturation of colors. The result of this operation, along with some artefacts, is visible in Figure 7(b). Again, the proposed method makes it possible to attenuate color blotches and to restore lost details (as can be seen *e.g.* on the patterns on the roofs in Figure 7(c)).

2) Comparison with other approaches: Two results of the regraining approach [5], respectively on the Renoir/Gauguin experiment and on a Lena/Barbara color transfer, are shown respectively on Figures 8(a) and 8(g). While this variational

(a) Original image. (b) Edited image. (c) Color correction with the proposed iterated TMR filter.

Fig. 7. **Illustration of image editing correction with iterated TMR filter.** (see electronic version of this paper). In this example, an image 7(a) is edited with an image editing software (The Gimp) for color enhancement (Figure 7(c)), using global contrast and saturation modification tools. Figure 7(c) displays the result of the proposed approach.

approach tends to reduce irregularities in the transportation map, it fails at removing severe compression artefacts or inconsistencies in color proportions. As a comparison, the result of the iterated TMR filter on both examples can be seen on Figures 8(b) and 8(h).

Another variational approach has been proposed very recently to transfer color between images without creating artefacts [10]. The result of this approach for the Renoir/Gauguin experiment is displayed in Figure 8(c), and for the Lena/Barbara color transfer in Figure 8(i). The method achieves the transfer without producing unpleasant artefacts, even if the color fidelity to the target distribution is not fully respected (*e.g.* the feather on the hat is purple whereas this color does not appear in Figure 8(e)).

D. Discussion

Patch-based regularization: Following the idea of the NL-means filter [21], one could think of replacing the pixel-wise comparisons in the TMR filter by patch comparisons. Indeed, in [21], Buades *et al.* show that using small patches instead of pixels increases the confidence level on the similarity measure between pixels corrupted by noise. In our case, it boils down to replace the weights in Formula (4) by

$$\hat{w}_u(x,y) = \exp\left(-\frac{\sum_{z\in W}\|u(x+z)-u(y+z)\|^2}{n\sigma^2}\right),$$

where W is a centered square neighborhood defined on the pixel grid, and where n is the size of W. Using patches in our framework does not improve the results (see Figure 9(e) for a comparison). On the contrary, using the same parameter σ, some fine structures are more blurred (along edges or stokes) with this approach, while some artefacts are less regularized (see the compression artefacts around the book title). Indeed, the use of patches tends to increase the similarity between pixels *across edges*, so that even some contrasted structures are blurred after several iterations. At the same time, the use of patches tends to decrease the similarity of pixels of non-repetitive structures (see [30] for details), which explains that some artefacts remain. While Yaroslavsky filter is less robust than the NL-means for denoising purposes, it is particularly adapted in our case, where the image u is regular. It permits a faster approach and a better preservation of edges.

Median-based regularization: In some cases, it could be interesting to replace Yaroslavsky filter by a median filter. Indeed, the median filter is parameter-less, it does not introduce blur and it is able to remove small objects (for instance salt and pepper noise). In the case of contrast modifications, Formula (5) can be rewritten as

$$\text{TMR}_u(T(u)) = \text{Med}_u\big(T(u)\big) + \ u - \text{Med}_u(u)\ ,$$

where $[\text{Med}_u(v)](x)$ is the weighted median of the values $v(y)$ when y spans $\mathcal{N}(x)$, with weights $\frac{w_u(x,y)}{C(x)}$. Figure 9(d) displays an example of the median based TMR filter. The result presents typical characteristics of median filter approaches, avoiding blurring effects that are inherent to averaging filters, while providing some unsatisfactory piece-wise constant regions.

V. Conclusion

In this paper, we have introduced a generic filtering procedure in order to remove the different kinds of artefacts created by radiometric or color modifications. The ability of the proposed TMR filter to deal these artefacts while restoring the fine details of images has been demonstrated on various examples.

Several extensions of this work are foreseen. First, notice that the computation time of the TMR operator is similar to those of the Bilateral filter [27] or Non-Local means [21]. As a consequence, it could directly benefit from several accelerations techniques that have been proposed recently in the literature for those type of filters, as for instance, multi-scale approximations [31], the use of kd-tree structures for fast computation of pixels comparison [32], or FFT-based convolutions [33]. Second, the whole procedure would also be strengthened by the automatic estimation of the parameters σ and ρ (for instance, by considering the recent work of [30]), even if most experiments gives satisfactory results running the same parameter values. Last, we plan to increase the control of color inconsistencies. Indeed, the approach presented here permits to remove artefacts due to color proportions as long as these are not too extreme. But it cannot completely modify the proportions of colors in the final image. In the case of color transfer, one possible option would be to transfer colors from a

(a) Color transfer with regraining [5]. (b) Color transfer with our approach. (c) Color transfer with approach of [10].

(d) Original image. (e) Target color distribution. (f) Raw color transfer.

(g) Regraining [5]. (h) Iterated TMR filter. (i) Color transfer with approach of [10].

Fig. 8. **Comparative color transfer regularization results** with regraining approach of [5] (Figures 8(a) and 8(g)), iterated TMR filter (Figures 8(b) and 8(h)) and variational histogram equalization of [10] (Figures 8(c) and 8(i)). Original images are shown respectively in Figures 6(g) and 8(d), with the corresponding target color distribution displayed respectively in Figures 6(h) and 8(e).

pre-computed "color palette" [6], [34]. We also believe that the scheme presented in this paper can benefit other applications that color or contrast modifications. One possible framework of application, for which the approach should of course be adapted, is the one of the fusion of panchromatic and multi-spectral images [35].

REFERENCES

[1] A. C. Bovik, *Handbook of Image and Video Processing (Communications, Networking and Multimedia)*. Orlando, FL, USA: Academic Press, Inc., 2005.

[2] C. Villani, *Topics in optimal transportation*. American Math. Soc., 2003.

[3] E. Reinhard, M. Ashikhmin, B. Gooch, and P. Shirley, "Color transfer between images," *IEEE Comput. Graph. Appl.*, vol. 21, no. 5, pp. 34–41, 2001.

[4] J. Morovic and P. Sun, "Accurate 3d image colour histogram transformation," vol. 24, no. 11, pp. 1725–1735, July 2003.

[5] F. Pitié, A. Kokaram, and R. Dahyot, "Automated colour grading using colour distribution transfer," *Computer Vision and Image Understanding*, February 2007.

[6] Y.-W. Tai, J. Jia, and C.-K. Tang, "Local color transfer via probabilistic segmentation by expectation-maximization," in *Proceedings of the IEEE Computer Society Conference on Computer Vision and Pattern*

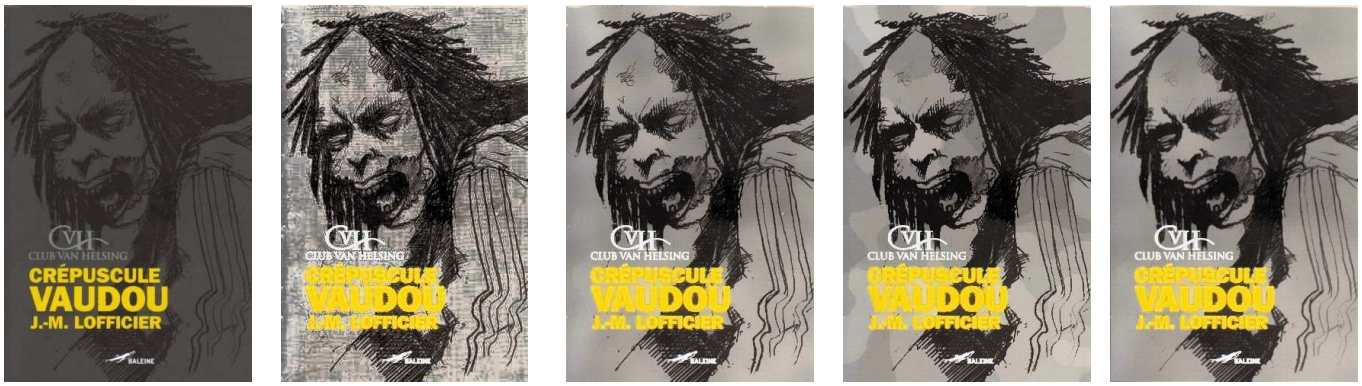

(a) Original image u (b) Histogram equalization (c) Proposed approach: Iterated TMR using Y_u filter (d) Extension: Iterated TMR using Median filter (e) Extension: Iterated TMR using Non-local filter

Fig. 9. **Variation around TMR filter based on different edge-preserving filters.** Figure 9(c): Yaroslavsky-based filter. Figure 9(d): Median-based filter. Figure 9(e): Non-local Means based filter with 3×3 pixels patches comparison. The same number of iterations (10) and the same parameter setting ($\sigma = 10$) have been used for each experiment.

Recognition (CVPR). Washington, DC, USA: IEEE Computer Society, 2005.

[7] R. Selzer, "The use of computers to improve biomedical image quality," Caltech, Tech. Rep., 1968.

[8] A. Rosenfeld and E. Troy, "Visual texture analysis," in *Proc. UMR-Kelly Comm. Conf.*, 1970.

[9] J. Delon, "Midway image equalization," *JMIV*, vol. 21, no. 2, pp. 119–134, September 2004.

[10] Papadakis, N. and Provenzi, E. and Caselles, V., "A Variational Model for Intermediate Histogram Equalization of Color Images," http://sites.google.com/site/nicolaspapadakis/Home/histo, 2010.

[11] J. Delon, "Movie and video scale-time equalization application to flicker reduction," *IP*, vol. 15, no. 1, pp. 241–248, 2006.

[12] J. Delon and A. Desolneux, "Flicker stabilization in image sequences," *Preprint HAL*, 2009.

[13] G. Haro, M. Bertalmío, and V. Caselles, "Visual acuity in day for night," *International Journal of Computer Vision*, vol. 69, no. 1, pp. 109–117, 2006.

[14] M. Bertalmío, V. Caselles, E. Provenzi, and A. Rizzi, "Perceptual color correction through variational techniques," *IEEE Transactions on Image Processing*, vol. 16, no. 4, pp. 1058–1072, 2007.

[15] S. G. Narasimhan and S. K. Nayar, "Vision and the atmosphere," *Int. J. Comput. Vision*, vol. 48, no. 3, pp. 233–254, 2002.

[16] L. A. Torres-Méndez and G. Dudek, "Color correction of underwater images for aquatic robot inspection," in *Energy Minimization Methods in Computer Vision and Pattern Recognition*, 2005, pp. 60–73.

[17] U. Lipowezky, "Grayscale aerial and space image colorization using texture classification," *Pattern Recogn. Lett.*, vol. 27, no. 4, pp. 275–286, 2006.

[18] S. M. Pizer, E. P. Amburn, J. D. Austin, R. Cromartie, A. Geselowitz, T. Greer, B. T. H. Romeny, and J. B. Zimmerman, "Adaptive histogram equalization and its variations," *Comput. Vision Graph. Image Process.*, vol. 39, no. 3, pp. 355–368, 1987.

[19] A. Abadpour and S. Kasaei, "An efficient pca-based color transfer method," *J. Vis. Comun. Image Represent.*, vol. 18, no. 1, pp. 15–34, 2007.

[20] F. Alter, S. Durand, and J. Froment, "Adapted total variation for artifact free decompression of jpeg images," *Journal of Math. Imaging and Vision*, vol. 23, pp. 199–211, 2005.

[21] A. Buades, B. Coll, and J. M. Morel, "A review of image denoising algorithms, with a new one," *Multiscale Modeling & Simulation*, vol. 4, no. 2, pp. 490+, 2005.

[22] L. Yaroslavsky, *Digital Picture Processing, An Introduction*. Berlin: Springer-Verlag, 1985.

[23] F. Durand and J. Dorsey, "Fast bilateral filtering for the display of high-dynamic-range images," in *Proc. of SIGGRAPH '02*. ACM, pp. 257–266.

[24] V. Caselles, B. Coll, and J.-M. Morel, "Topographic maps and local contrast changes in natural images," *Int. J. Comput. Vision*, vol. 33, no. 1, pp. 5–27, 1999.

[25] J. Rabin, G. Peyré, J. Delon, and M. Bernot, "Wasserstein Barycenter and its Application to Texture Mixing," http://hal.archives-ouvertes.fr/hal-00476064/en/, 2010.

[26] S. M. Smith and J. M. Brady, "SUSAN—A New Approach to Low Level Image Processing," *Int. J. Comput. Vision*, vol. 23, no. 1, pp. 45–78, 1997.

[27] C. Tomasi and R. Manduchi, "Bilateral filtering for gray and color images," in *Proc. of ICCV '98*, p. 839.

[28] E. Eisemann and F. Durand, "Flash photography enhancement via intrinsic relighting," *ACM Trans. Graph.*, vol. 23, no. 3, pp. 673–678, 2004.

[29] J. Delon and A. Desolneux, "Stabilization of flicker-like effects in image sequences through local contrast correction," 2009. [Online]. Available: http://hal.archives-ouvertes.fr/hal-00407796/en/

[30] V. Duval, J.-F. Aujol, and Y. Gousseau, "On the parameter choice for the Non-Local Means," http://hal.archives-ouvertes.fr/hal-00468856/en/, 2010.

[31] C. Kervrann and J. Boulanger, "Local adaptivity to variable smoothness for exemplar-based image denoising and representation," *International Journal of Computer Vision*, vol. 79, no. 1, pp. 45–69, August 2008.

[32] A. Adams, N. Gelfand, J. Dolson, and M. Levoy, "Gaussian KD-trees for fast high-dimensional filtering," vol. 28, no. 3. ACM, pp. 1–12.

[33] J. Darbon, A. Cunha, T. Chan, S. Osher, and G. Jensen, "Fast nonlocal filtering applied to electron cryomicroscopy," in *In the proceedings of the IEEE International Symposium on Biomedical Imaging (ISBI'08)*, 2008.

[34] J. Delon, A. Desolneux, J. L. Lisani, and A. B. Petro, "Automatic color palette," *Inverse Problems and Imaging*, vol. 1, no. 2, pp. 265–287, 2007.

[35] C. Ballester, V. Caselles, L. Igual, J. Verdera, and B. Rougé, "A variational model for p+xs image fusion," *Int. J. Comput. Vision*, vol. 69, no. 1, pp. 43–58, 2006.

[36] G. Monge, *Mémoire sur la théorie des déblais et des remblais*. Histoire de l'Académie Royale des Sciences, 1781.

[37] P. Brémaud, *Markov chains: Gibbs field, Monte Carlo simulation and queues*. Springer New York, 1999.

[38] E. Seneta, *Non-negative Matrices and Markov Chains*, ser. Springer Series in Statistics. Springer-Verlag, 1973.

APPENDIX A
LINK WITH OPTIMAL TRANSPORT

This section recalls why color ans contrast transfers can be seen as optimal transportation problems. As described in Section II-B, assigning a given distribution f to an image u boils down to find a mapping T such that $h_{T(u)} = f$. If such mappings exist, one looks generally for one minimizing the global cost

$$\int_{\mathbb{R}^n} \|T(x) - x\|^2 h_u(dx) \, , \tag{8}$$

where $\|.\|$ is the Euclidean norm. This problem, first stated by Monge in [36], has generally no solution when h_u is discrete. Kantorovich proposed to relax the problem into a more general one, where one looks for a probability distribution π on $\mathbb{R}^n \times \mathbb{R}^n$, with marginals h_u and f (we write $\Pi(h_u, f)$ the set of these probability measures, which are called transportation plans). Observe that π can be seen as a multivalued function sending exactly h_u onto f. Among all transportation plans in $\Pi(h_u, f)$, one imposes that π minimizes a global transportation cost

$$\int_{\mathbb{R}^n \times \mathbb{R}^n} \|x - y\|^2 \pi(dx \times dy). \tag{9}$$

In practice, a satisfying mapping T between h_u and f can then be chosen as one approximating the optimal plan π. If we apply this framework to the case $n = 1$, we find formulas similar to (3) for histogram equalization and specification.

APPENDIX B
POWERS OF STOCHASTIC MATRICES

In this section, we recall the Perron-Frobenius theorem as it is stated in [37], [38]. Recall that a square matrix A is said to be *primitive* if there exists $q \in \mathbb{N}^*$ such that A^q is strictly positive, in the sense that all coefficients $A^q_{i,j}$ are strictly positive.

Theorem 1 (Perron-Frobenius, see [37], [38]): Let A be a nonnegative primitive $m \times m$ matrix. There exists a real eigenvalue λ_1 with algebraic as well as geometric multiplicity one such that $\lambda_1 > 0$, and $\lambda_1 > |\lambda_j|$ for any other eigenvalue λ_j. Moreover, the left eigenvector π_1 and the right eigenvector l_1 associated with λ_1 can be chosen positive and such that $\pi_1^T l_1 = 1$. Let $\lambda_2, \lambda_3, \dots \lambda_m$ be the eigenvalues of A other than λ_1 ordered in such a way that $\lambda_1 > |\lambda_2| \geq \cdots \geq |\lambda_m|$ and if $|\lambda_2| = |\lambda_j|$ for some $j \geq 3$, then $m_2 \geq m_j$, where m_j is the algebraic multiplicity of λ_j. Then,

$$A^r = \lambda_1^r l_1 \pi_1^T + O(r^{m_2 - 1} |\lambda_2|^r), \tag{10}$$

where $O(f(r))$ represents a function of r such that there exists $\alpha, \beta \in \mathbb{R}$, $0 < \alpha \leq \beta < \infty$, such that $\alpha f(r) < O(f(r)) < \beta f(r)$ for all r sufficiently large.

Proof: see [38].

Observe that the matrix A defined in Section III-C is stochastic, which implies that $\lambda_1 = 1$ and $l_1 = (1, 1, \dots, 1)^T$. All the lines of A^∞ are thus equal to the left eigenvector π_1 for the eigenvalue 1. Now, if the neighborhood $\mathcal{N}(0)$ is symmetric (which implies that $i \in \mathcal{N}(j)$ if and only if $j \in \mathcal{N}(i)$), this left eigenvector is

$$\pi_1(i) = \left(\sum_{j=1}^{m} w_u(i,j).\mathbb{1}_{j \in \mathcal{N}(i)} \right) / \left(\sum_{k,j=1}^{m} w_u(k,j).\mathbb{1}_{j \in \mathcal{N}(k)} \right),$$

where exponential weights w_u are defined in Formula 4. The limit matrix can thus be computed easily in this case.

APPENDIX C
STOCHASTIC MATRICES WITH STOPPING CRITERION

In the following, we show that if A is the matrix defined in Section III-C, and if B is built by replacing some lines in A by the same lines in the identity matrix, then the sequence (B^k) still converges toward a limit matrix B^∞. This property is a consequence of classical results and the proof is provided for the sake of completeness.

First, observe that there exists a permutation matrix Σ such that $B' = \Sigma B \Sigma^{-1}$ can be written

$$\begin{pmatrix} I_r & \mathbf{0}_{r \times (m-r)} \\ R & Q \end{pmatrix}, \tag{11}$$

where I_r is the identity matrix of size r, $\mathbf{0}_{r \times (m-r)}$ is the null matrix of size $r \times (m-r)$, $R \in \mathcal{M}_{m-r,r}(\mathbb{R})$ and $Q \in \mathcal{M}_{m-r}(\mathbb{R})$. Since $B^k = \Sigma^{-1} B'^k \Sigma$, the convergence of the sequence (B'^k) will imply the convergence of (B^k), so we assume in the following that B is written as in (11). Now,

$$B^k = \begin{pmatrix} I_r & \mathbf{0}_{r \times (m-r)} \\ R_k & Q^k \end{pmatrix}, \text{ with } R_k = \left(\sum_{j=0}^{k-1} Q^j \right) R, \tag{12}$$

and the study of the sequence (B^k) boils down to the study of the sequence (Q^k).

Now, observe that the sequence $\sum_{j=1}^{m-r} (Q^k)_{i,j} = \sum_{j=r+1}^{m} (B^k)_{i+r,j}$ decreases with k, for all $1 \leq i \leq m-r$. Indeed, since B is stochastic, for all i,

$$\sum_{j=1}^{m-r} (Q^{k+1})_{i,j} = \sum_{j=1}^{m-r} \sum_{l=1}^{m-r} (Q^k)_{i,l} Q_{l,j} \leq \sum_{l=1}^{m-r} (Q^k)_{i,l} .$$

Moreover, for each line $i \leq m-r$, there exists a rank k_0 such that for all $k \geq k_0$, $\sum_{j=1}^{m-r} (Q^k)_{i,j} < 1$. Indeed, the set $\mathcal{C}$ of points which have already converged is not isolated in the image. Step by step, each point outside of $\mathcal{C}$ (indexes $\{r+1, \dots m\}$ in B) undergoes the influence of at least one point of $\mathcal{C}$ (indexes $\{1, \dots r\}$ in B) after a large enough number of iterations, which implies that for all $i \in \{r+1, \dots m\}$, there exists k_0 and $j \in \{1, \dots r\}$ such that $R_k(i,j) > 0$ for $k \geq k_0$.

The index k_0 can be chosen such that this property holds for all $i \in \{1, \dots, m-r\}$. Since these sequences are decreasing, there exists γ in $]0,1[$ such that for all i and all $k > k_0$, $\sum_{j=1}^{m-r} (Q^k)_{i,j} < \gamma$. Thus, for each $p \in \mathbb{N}^{+*}$,

$$\begin{aligned} \sum_{j=1}^{m-r} (Q^{pk+k})_{i,j} &= \sum_{j=1}^{m-r} \sum_{l=1}^{m-r} (Q^{pk})_{i,l} (Q^k)_{l,j} \\ &\leq \gamma \sum_{l=1}^{m-r} (Q^{pk})_{i,l} < \gamma^{p+1} . \end{aligned}$$

It follows that $\sum_{j=1}^{m-r} (Q^{pk})_{i,j} \underset{p \to \infty}{\to} 0$. This property also holds for the whole sequence $\sum_{j=1}^{m-r} (Q^k)_{i,j}$ since it is decreasing with a subsequence converging to 0. Since all the coefficients of these matrices are positive, we conclude that $Q^k \underset{k \to \infty}{\to} 0$.

Now, notice that $R_k = \left(\sum_{j=0}^{k-1} Q^j \right) R = (I - Q)^{-1} (I - Q^k) R$ (if $I - Q$ was not invertible, then we would have $x \neq 0$

such that $Qx = x$ which is impossible since $Q^k \underset{k\to\infty}{\to} 0$). Thus $R_k \underset{k\to\infty}{\to} (I-Q)^{-1}R$. Finally,

$$B^k \underset{k\to\infty}{\longrightarrow} \begin{pmatrix} I_r & \mathbf{0}_{r\times(m-r)} \\ (I-Q)^{-1}R & \mathbf{0}_{(m-r)\times(m-r)} \end{pmatrix}. \quad (13)$$

■

ACKNOWLEDGMENT

The authors are grateful to acknowledge Adrian Márques for its work on flicker experiments. The authors would like also to thank Gabriel Peyré for its fruitful comments and discussions. This work has been supported by the French National Research Agency (project ANR-07-BLAN-0235 OTARIE, project ANR-07-JCJC-0048 FREEDOM and ANR-09-CORD-003 CALLISTO).